Mapping Gold-Bearing Massive Sulfide Deposits in the Neoproterozoic Allaqi Suture, Southeast Egypt with Landsat TM and SIR-C/X SAR Images

Talaat M. Ramadan, Mohamed G. Abdelsalam, and Robert J. Stern

Abstract

*Meta-volcanic sequences in the Neoproterozoic Arabian-Nubian Shield host auriferous massive sulfide deposits with surface expression in the form of clay and iron alteration zones. These are large enough (few hundreds of meters across) and have distinctive characteristic reflectance spectra to be mapped with the 30-m spatial resolution Landsat Thematic Mapper (TM) images. Landsat TM together with Shuttle Imaging Radar (SIR)-C/X-Synthetic Aperture Radar (SAR) images are used for finding and mapping the alteration zones in the western part of the east-trending Allaqi suture in the Southeastern Desert of Egypt. The 5/7-5/1-3/4*5/4 band-ratio Landsat TM image shows the Umm Garaiat alteration zone as sugary white; this appears red in the 5/7-4/5-3/1 band-ratio Landsat TM image. Geological and geochemical data indicate that the Umm Garaiat alteration zone is the surface expression of a massive sulfide deposit that contains up to 12 g/t gold. Density slicing using 5/7 and 3/1 Landsat TM band-ratios effectively maps clay and iron alteration. The 5/7 density slicing Landsat TM image suggests that the Umm Garaiat alteration zone is dominated by clay minerals. The 3/1 density slicing Landsat TM image shows little evidence for FeO minerals associated with the Umm Garaiat alteration zone. Analysis of Landsat TM images with supervised classification techniques using the Umm Garaiat alteration zone as the training site helped identify previously unknown alteration zones at Wadi Marahiq. Interpretation of Chh-Lhh-Lhv SIR-C/X-SAR images helped in understanding the lithological and structural controls on massive sulfide deposits in the study area. This demonstrates the utility of orbital remote sensing for finding ore deposits in arid regions.*

Introduction

The Wadi Allaqi area lies in the Southeastern Desert of Egypt and represents part of the Neoproterozoic Arabian-Nubian Shield (Figure 1). The region is dominated by the western extension of the Allaqi-Heiani-Gerf-Onib-Sol Hamid-Yanbu suture (Stern *et al.*, 1989; Stern, 1994; Abdelsalam and Stern, 1996a; Figure 1). In the Wadi Allaqi area, the suture is defined by deformed and metamorphosed ophiolitic fragments, supracrustal sequences, and intrusive rocks which host gold-bearing massive sulfide deposits and auriferous quartz veins (Figure 2).

Massive sulfide deposits are rarely exposed, but distinctive iron oxide and clay zones of hydrothermal alteration associated with these deposits are exposed (Sato, 1974; Kearey, 1993). These have distinctive surface expression that can be identified using orbital remote sensing images. This study presents the first attempt to use Landsat TM and SIR-C/X-SAR images to identify and map alteration zones in the Neoproterozoic basement of Egypt. We also used the images to infer lithological and structural controls on massive sulfide deposits.

Tectonic Setting

The Neoproterozoic basement rocks in northeastern Africa and eastern Arabia comprise the Arabian-Nubian Shield (Figure 1), which is made up of intra-oceanic island-arc and back-arc-basin complexes and micro-continents welded together along north- to east-trending sutures and disrupted by north- and northwestern-trending post-accretionary shear zones (Stern, 1994; Abdelsalam and Stern, 1996). One of these sutures is the east- to northeast-trending Allaqi-Heiani-Onib-Sol Hamed-Yanbu suture (Stern *et al.*, 1990). The western part of this suture is exposed north of Wadi Allaqi (Figures 1 and 2) and is the focus of this study. The suture in northeastern Sudan and southeastern Egypt separates the Southeastern Desert terrane in the north from the 830 to 720-Ma Hijaz-Gebeit-Gabgaba-Halfa terrane to the south (Figure 1).

Geology

The Wadi Allaqi area is underlain by Neoproterozoic crystalline rocks, Cretaceous sandstone, and Mesozoic and younger volcanic and sub-volcanic rocks. The Neoproterozoic rocks and associated gold-bearing massive sulfide deposits are the focus of this study. These rocks underlie most of the study area and consist of ophiolitic assemblage, island arc assemblage, and late- to post-tectonic granitic intrusions (Figure 2). These, together with the massive sulfide deposits and associated alteration zones, are discussed below.

The Ophiolitic Assemblage

These rocks are scattered in the central part of the Wadi Allaqi area (Figure 2) and are made up of imbricated thrust sheets

T. M. Ramadan is with the National Authority for Remote Sensing and Space Sciences, Cairo, Egypt.

M.G. Abdelsalam and R.J. Stern are with the Center for Lithospheric Studies, University of Texas at Dallas, Richardson, TX 75083-0688 (abdels@utdallas.edu).

Photogrammetric Engineering & Remote Sensing
Vol. 67, No. 4, April 2001, pp. 491–497.

0099-1112/01/6704–491$3.00/0

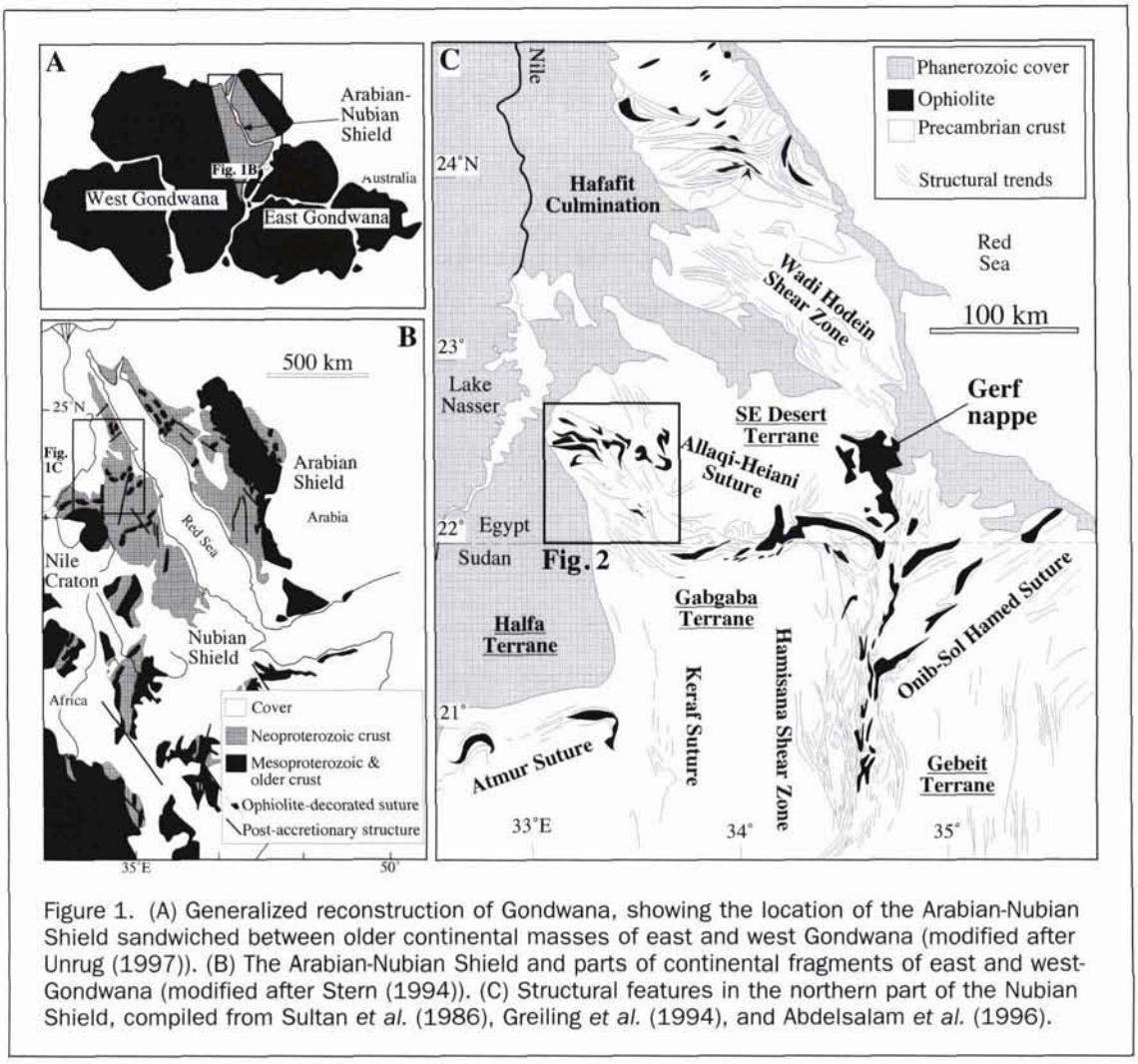

Figure 1. (A) Generalized reconstruction of Gondwana, showing the location of the Arabian-Nubian Shield sandwiched between older continental masses of east and west Gondwana (modified after Unrug (1997)). (B) The Arabian-Nubian Shield and parts of continental fragments of east and west-Gondwana (modified after Stern (1994)). (C) Structural features in the northern part of the Nubian Shield, compiled from Sultan *et al.* (1986), Greiling *et al.* (1994), and Abdelsalam *et al.* (1996).

and slices of serpentinites, talc carbonate schist, and meta-gabbros. These are thrust from north to south across the island-arc assemblage (Figure 2). The serpentinites are distinguished by their characteristic red color in the 5/7-5/1-3/4*5/4 Landsat TM image (labeled **SP** in Figure 3B). Talc-carbonate schists typically define the contact between the serpentinites and meta-sedimentary and meta-volcanic rocks of the island-arc assemblage and are identifiable on the 5/7-5/1-3/4*5/4 Landsat TM image by their sugary white color (labeled **TA** in Figure 3B).

The Island-Arc Assemblage

This assemblage is represented by meta-sedimentary and meta-volcanic layered units and intrusive gabbro to diorite plutons (Figure 2). The geochemistry of some of these meta-volcanic rocks suggests transitional environment between continental arc and continental margin (El-Nisr, 1997). The clastic meta-sedimentary units appear purple in the 5/7-5/1-3/4*5/4 Landsat TM image (labeled **MS** in Figure 3B). Meta-volcanic rocks of intermediate to mafic composition dominate the study area south of Wadi Shelman (Figure 2). These meta-volcanic rocks appear bluish in the 5/7-5/1-3/4*5/4 Landsat TM image (labeled **MV** in Figure 3B). These meta-volcanics host the gold-bearing massive sulfide deposits and associated alteration zones in the Wadi Umm Garaiat and Wadi Marahiq areas (Figure 2). Ancient ruins and artifacts such as grinding stones indicate that the Umm Garaiat and Marahiq gold deposits were mined since Pharonic times.

The gabbro-diorite intrusions of the island-arc assemblage are less abundant than the meta-sedimentary and meta-volcanic units. These intrusions are heterogeneous in composition and include gabbro, diorite, quartz-diorite, and tonalite. The gabbroic intrusions appear as bluish circular bodies in 5/7-5/1-3/4*5/4 Landsat TM image (labeled **SG** in Figure 3B).

The Late- to Post-Tectonic Granitoids

Late- to post-tectonic granitic bodies are widespread in the central part of the study area, especially close to Wadi Umm Shelman (Figure 2). They occur as deeply eroded, circular features with few isolated low-lying hills draped by Recent sand deposits (labeled **PG** in Figure 3B). The characteristically circular appearance of granitoids makes it easy to distinguish them in the Chh-Lhh-Lhv SIR-C/X-SAR image (labeled **PG** in Figure 3C). In the northern part of the Wadi Marahiq area, a large, late-tectonic pluton intrudes meta-volcanic rocks (Figure 2). This pluton comprises medium- to coarse-grained granite with disseminated pyrite, chalcopyrite, and malachite. The pluton is surrounded by the Umm Garaiat and Marahiq alteration zones (Figure 2) and might be related to the massive sulfide deposits in the study area.

Post-tectonic granitic bodies are widely distributed in the northern part of the study area (Figure 2). They are massive, medium in grain size, and red in color with high to medium relief. They intruded the above rock unites and are cut by felsic intrusions as well as felsic and mafic dikes.

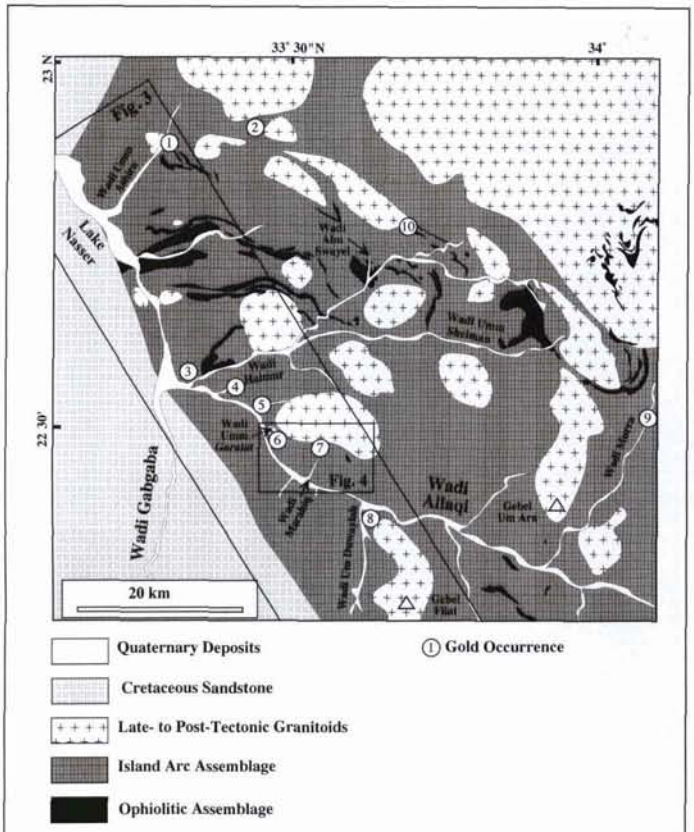

Figure 2. Regional geologic map of the western part of the Allaqi suture based on interpretation of 5/7-5/1-3/4*5/4 Landsat TM image. Circled numbers indicate named gold mines reported in Hume (1937). 1 = Umm Ashira, 2 = Hariari, 3 = Haimur, 4 = Nile Valley, 5 = Umm Garaiat, 6 = Marahiq, 7 = Atshani, 8 = Filat, 9 = Murra, and 10 = Neqib.

The Massive Sulfide Deposits and Associated Alteration Zones

Hydrothermally altered zones are widely distributed in the Wadi Allaqi area. These are characterized by kaolitization, silicification, and ferrugonation, which is characteristic for alteration zones on top of massive sulfide deposits (Sato, 1974; Kearey, 1993). This and previous field studies revealed the presence of several alteration zones in the Wadi Umm Garayat and Wadi Marahiq areas (Figure 2).

The Umm Garaiat Alteration Zone

This alteration zone is located about 22°33′N and 33°27′E (Figure 2), and is associated with meta-andesites and meta-dacites which are intruded by gabbro-diorite (Hussein, 1990). Some of the gabbro-diorite plutons might be related to the massive sulfide deposits. The largest of these alteration zones occurs about 3 km southeast of Umm Garaiat gold mine (Figure 2) which was active in ancient times and in the early 20th century (Hume, 1937). The Umm Garaiat alteration zone (labeled **1** in Figures 4B and 4C) is characterized by a silicified core that is rimmed by concentric zones dominated by pyrophyllitization, alunitization, and ferrugenization. Within the silicified core, minor quartz veins with apatite, tourmaline, and occasional specks of gold are encountered. A pronounced magnetic anomaly coincides with this alteration zone, suggesting that an ore deposit might be buried beneath the alteration zone (Hussein, 1990). A 212-meter-deep bore hole drilled by the Egyptian Geological Survey in 1991 confirmed that a large pyrite-bearing massive sulfide deposit lay beneath a 70-meter-thick alteration zone. Moreover, gold-bearing quartz veins are present north and south of the alteration zone. Analyses of 15 quartz vein samples from south of the alteration zone indicate between 0.3 and 3 g/t gold and between 1.5 and 6 g/t silver.

The Marahiq Alteration Zone

This alteration zone is located near 22°30′N and 33°30′E (Figure 2). Meta-volcanic rocks of the island-arc assemblage host the alteration zone. These meta-volcanic rocks are composed of pillowed meta-basalts, meta-andesites, and meta-dacites, and host the gold-bearing massive sulfide deposits. North of the alteration zone, a small ophiolite-related talc schist body (labeled **TA** in Figure 4A) is imbricated with the meta-volcanic rocks. A circular granodioritic pluton intrudes the meta-volcanic rocks. The granodiorite is medium- to coarse-grained and frequently contains disseminated pyrite, chalcopyrite, and malachite. The alteration zones (Figure 4H) surround this pluton, and it is thought that it might be related to these massive sulfide deposits.

There are four distinct northwest-elongated alteration zones on the eastern side of Wadi Marahiq (labeled **2**, **3**, **4**, and **5** in Figures 4B and 4C). The two alteration zones that lie just east of Wadi Marahiq (labeled **2** and **5** in Figures 4B and 4C) have been studied previously in the field, and the north one (labeled **5** in Figures 4B and 4C) is an ancient mine named Atshani (Hume, 1937). The southern alteration zone (labeled **2** in Figures 4B and 4C) near the mouth of Wadi Marahiq forms a circular structure about 400 meters in diameter. The composition of the Marahiq alteration zones is similar to that of Umm Garaiat, with intensely silicified and sericitized cores that are surrounded by kaolintized zones. Pyrite crystals up to 2 cm across have grown superimposed on these alterations and pyritization is characteristic of the transitional zones between altered and unaltered rocks. Northwest-trending gold- and pyrite-bearing quartz veins are present within the alteration zones and reach up to 20 m long and 30 cm wide. Chemical analysis for 25 representative samples from the alteration zones and the associated quartz veins reveal that the quartz veins contain between 0.3 and 12 g/t gold and the alteration zone has 0.3 to 0.9 g/t gold concentration. The pyrites contain up to 1.5 g/t gold. The two eastern alteration zones (labeled **3** and **4** in Figures 4B and 4C) are interpreted by us from analysis of Landsat TM images, as discused below. The northeastern alteration zone (labeled **4** in Figures 4B and 4C) was suspected on the basis of reconnaissance studies, but the southeastern body (labeled **3** in Figures 4B and 4C) is a suspected discovery.

Remote Sensing Analysis

Landsat TM and SIR-C/X-SAR images were used to map the alteration zones associated with the massive sulfide deposits as well as to help understand their lithological and structural controls. Previous remote sensing studies in the area includes visual interpretation of Landsat Multi-Spectral Scanner (MSS) and TM images for regional geologic investigation (El-Shazly *et al.*, 1983) and to aid for regional exploration for gold (El-Shazly *et al.*, 1986; El-Shazly *et al.*, 1988).

Landsat TM Images

We processed Landsat TM data to generate three red-green-blue (RGB) color-composite overlays for the western part of the Allaqi suture (Figures 3A and 3B) and the Umm Garaiat and Marahiq alteration zones (Figures 4A, 4B, and 4C):

(1) Normal-color images using band 3 as red, 2 as green, and 1 as blue (Figures 3A and 4A). These are referred to as 3-2-1 Landsat TM images.
(2) An "Abrams-type" image (Abrams *et al.*, 1983) using band-ratios 5/7 as red, 4/5 as green, and 3/1 as blue (Figure 4B). This is referred to as 5/7-4/5-3/1 Landsat TM image. Landsat

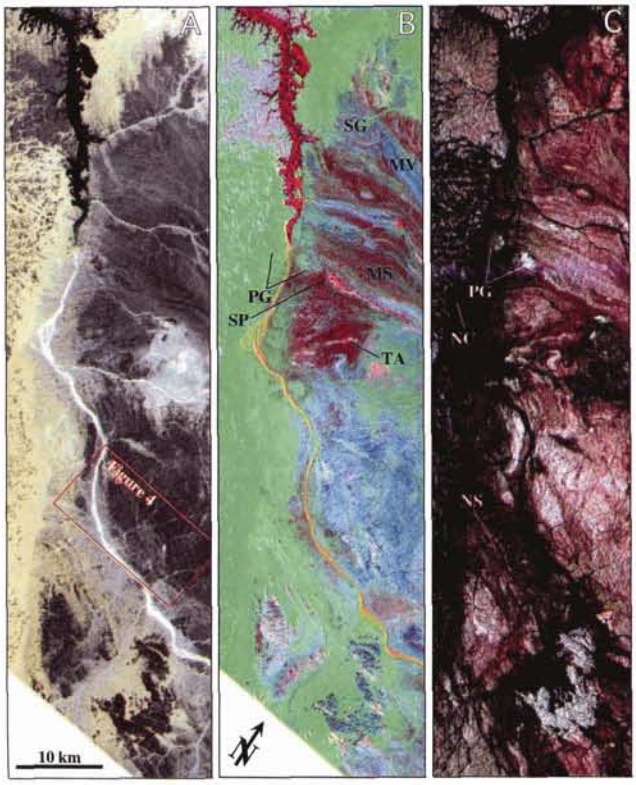

Figure 3. Comparison between (A) 3-2-1 Landsat TM image, (B) 5/7-5/1-3/4*5/4 Landsat TM image, and (C) Chh-Lhh-Lhv SIR-C/X-SAR image of the western part of the Allaqi suture. The comparison shows the power of band-ratio Landsat TM images in lithological identification of different rock types and the usefulness of SIR-C/X-SAR imagery in tracing Neoprotetozoic structures. **SP** = Serpentinite, **TA** = Talc schist, **MS** = Meta-sedimentary rock, **MV** = Meta-volcanic rock, **SG** = Gabbro-diorite intrusion of the island arc assemblage, **PG** = Late- to post-tectonic intrusion, **NS** = Neoproterozoic structure, and **NC** = Neoproterozoic basement/Cretaceous sandstone fault contact.

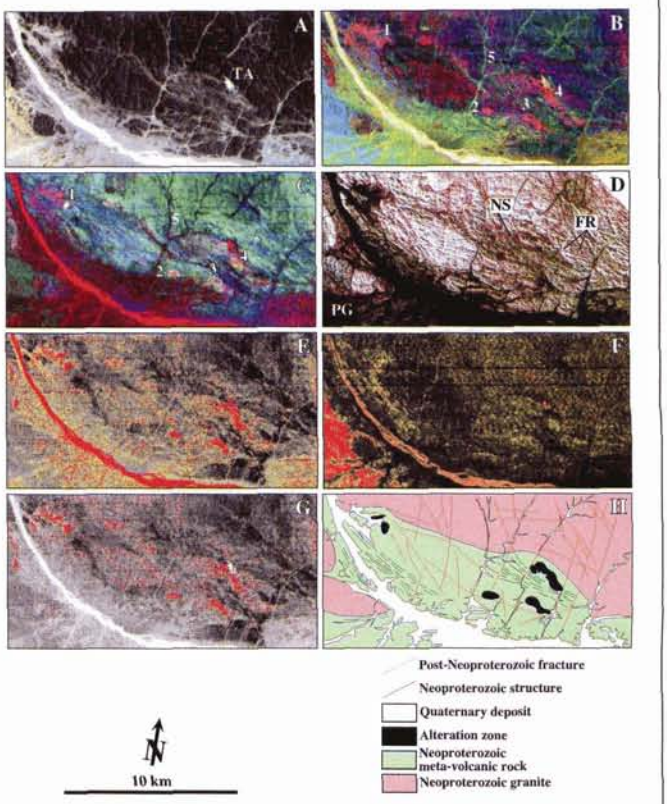

Figure 4. Remote sensing analysis of the Umm Garaiat and Marahiq alteration zones. (A) 3-2-1 Landsat TM image. (B) 5/7-4/5-3/1 Landsat TM image. (C) 5/7-5/1-3/4*5/4 Landsat TM image. (D) Chh-Lhh-Lhv SIR-C/X-SAR image. (E) Clay alteration index map draped over 5/7 Landsat TM image. The digital numbers (DNS) of the density slices are calculated to represent top ~5% (red), ~15% (orange), and ~25% (yellow). (F) Iron alteration index map draped over 3/1 Landsat TM image. The DNs of the density slices are calculated to represent the top ~50% (red), ~60% (orange), and 70% (yellow). (G) Results of parallelepiped supervised classification based on Landsat TM band-ratio 5/7 and 3/1 and using a cluster of 29 pixels coinciding with the Umm Garaiat alteration zone as a training site and a standard deviation from the mean of 2.5. (H) Geologic map of the Umm Garaiat and Marahiq alteration zones based on the remote sensing analysis shown in Figures 4A to 4G. **TA** = Talc schist. The numbers **1** to **5** indicate individual alteration zones. **1** = The Umm Garaiat alteration zone, and **2** to **5** = Marahiq alteration zones. **FR** = Post-Neoproterozoic fracture. **NS** = Neoproterozoic structure. **PG** = Late- to post-tectonic granite.

TM band-ratios 5/7, 4/5, and 3/1 are produced by dividing the digital number (DN) of one band by another to yield an image that enhances spectral differences and reduce the morphology effect. Landsat TM band-ratios 5/7 and 3/1 are used because clay and iron minerals have reflectance and absorption features in these bands, respectively (Sabins, 1997), as will be discussed later. Landsat TM band-ratio 4/5 is used because it emphasizes silicates minerals compared to FeO-rich minerals (Abrams *et al.*, 1983).

(3) Sultan-type images (Sultan *et al.*, 1986; Sultan *et al.*, 1987) using band-ratio 5/7 as red, 5/1 as green, and 3/4*5/4 as blue (Figures 3B and 4C). These are referred to as 5/7-5/1-3/4*5/4 Landsat TM images. Sultan *et al.* (1986; 1987) used the 5/7-5/1-5/4*3/4 Landsat TM images to map lithologies in the Eastern Desert of Egypt and found them useful for identifying ultramafic rocks. Landsat TM band-ratio 5/1 is used because magnetite and other opaque minerals have reflectance feature in band 5 and absorption feature in band 1 (Sultan *et al.*, 1987). This is similar to the Landsat TM band-ratio 3/1 used in the Abrams-type images (Abrams *et al.*, 1983). FeO-rich aluminosilicate minerals have reflectance features at bands 3 and 5 and absorption feature at band 4. Hence, band-ratios 3/4 and 5/4 result in high DN values in pixels dominated by FeO-rich aluminosilicates minerals. Multiplying 5/4 by 3/4 to yield 5/4*3/4 results in even higher DN values, hence better definition of these minerals (Sultan *et al.*, 1987).

The 3-2-1 Landsat TM image provides a synoptic overview of the study area that is useful for mapping regional morphological features such as wadis (dry rivers), bedrock outcrops, and sandy areas (Figures 3A and 4A). Moreover, this image is useful in identifying linear structures such as young faults and fractures because these have morphological expression (Figures 3A and 4A). In addition, this image shows the talc schist body as characteristically white (labeled TA in Figure 4A). This is due to high reflectance of the Landsat TM visible bands (band 3 = visible red, 2 = visible green, and 1 = visible blue) by the talc deposit.

The 5/7-4/5-3/1 (Figure 4B) and 5/7-5/1-3/4*5/4 Landsat

TM images (Figures 3B and 4C) are used to discriminate different rock types in the study area. More importantly, these images are useful in identifying the alteration zones. In the 5/7-4/5-3/1 Landsat TM image, these alteration zones (labeled **1**, **2**, **3**, **4**, and **5** in Figure 4B) appear red, suggesting the domination of clay minerals. In the 5/7-5/1-3/4*5/4 Landsat TM image, the alteration zones (labeled **1**, **2**, **3**, **4**, and **5** in Figure 4C) appear sugary white. This indicates a high digital number (DN) of the alteration zones for the 5/7, 5/1, and 3/4*5/4 Landsat TM band-ratios.

SIR-C/X-SAR Radar Images

Orbital imaging radar is not widely used to directly explore for massive sulfide deposits, although SAR data have been integrated with Landsat TM and geophysical data to understand lithological and structural controls on ore bodies (Rheault *et al.*, 1989; Harris *et al.*, 1989; Rowan and Bowers, 1995). Radar back-scattering is a function of surface roughness together with other environment- and system-related factors (Lewis *et al.*, 1998). Hence, radar can be used to map surficial deposits such as alluvial fans, lava flows, and glacial debris (Singhory *et al.*, 1989; Farr and Chadwick, 1996; Weeks *et al.*, 1996; Zebker *et al.*, 1996). In addition to surface roughness, radar back-scattering is affected by the dielectric properties of the imaged surfaces. This is largely controlled by the moisture content and to a lesser extent by the material composition (Lewis *et al.*, 1998). They concluded that the enhanced back-scattering from an imaged surface reflects the moisture content rather than composition. However, FeO-rich minerals have slightly elevated dielectric constants compared to other geologic material (Sabins *et al.*, 1997).

Massive sulfide deposits might be identifiable with radar if the associated alteration zones have distinctively rough surfaces and elevated dielectric constants. SIR-C/X-SAR images covering part of the Neoproterozoic terrane in northern Eritrea were successfully used to identify gossans associated with the Beddaho alteration zone (Abdelsalam *et al.*, 2000a). This is because these gossans have a rougher surface compared with the surrounding hydrothermally altered meta-sedimentary and meta-volcanic rocks (Abdelsalam *et al.*, 2000a).

SIR-C/X SAR images cover most of the western part of the Wadi Allaqi area (Figure 3C). We used a color-composite Chh-Lhh-Lhv SIR-C/X SAR image (Figure 3C) to compare it with Landsat TM images (Figures 3A and 3B) and to study structural features of the western Allaqi suture. Moreover, we selected a subset of the SIR-C/X-SAR image to cover the Umm Garaiat and Marahiq alteration zones (Figure 4D). In these images C-band (wavelength = 6 cm) horizontally transmitted and horizontally received (hh) is assigned to red, L-band (wavelength = 24 cm) horizontally transmitted and horizontally received (hh) is assigned to green, and L-band horizontally transmitted and vertically received (hv) is assigned to blue. Imaging with orbital radar systems depends on measuring the amplitude, time delay, and phase shifts of back-scattered radar signal (Zebker and Goldstein, 1986). Back-scattering is largely controlled by the perceived surface roughness relative to the radar band wavelength (Lewis *et al.*, 1998). Shorter wavelengths increased the perceived surface roughness (Campbell and Campbell, 1992). On the other hand, longer wavelengths and cross-polarization result in deeper radar penetration (Schaber *et al.*, 1997). Using radar bands with different wavelengths and polarization on the RGB color-composite overlay creates false colors that are reflective of the perceived surface roughness of the imaged surface which is governed by the weathering pattern of geologic materials (Lewis *et al.*, 1998) that is largely controlled by lithology. In addition, these false color images enable surface and shallowly buried (2 m) geologic features to be displayed in the same image. The Chh-Lhh-Lhv SIR-C/X-SAR images proved effective for geologic studies in arid regions, especially the eastern Sahara (Abdelsalam and Stern, 1996b; Abdelsalam *et al.*, 2000a; Abdelsalam *et al.*, 2000b).

The Chh-Lhh-Lhv SIR-C/X-SAR images reveal several features beneath the thin dry sand that obscures the underling bedrock from being imaged by the Landsat TM imagery. The granitic bodies that appear white in the SIR-C/X-SAR image (labeled **PG** in Figure 3C) but are not obvious in the Landsat TM images (compare Figure 3C with Figures 3A and 3B) best exemplify this. Similarly, the SIR-C/X-SAR image revealed the Neoproterzoic structure south of Wadi Allaqi (labeled **NS** in Figure 3C) better than the Landsat TM images (Figures 3A and 3B). In addition, the SIR-C/X-SAR image revealed the contact between the Neoproterozoic crystalline basement and the Cretaceous sandstone (labeled **NC** in Figure 3C) as sharp northnorthwest-trending linear feature which might be a normal fault with the Cretaceous sandstone occupying the hangingwall. This boundary is not obvious in the Landsat TM images.

In the Chh-Lhh-Lhv SIR-C/X-SAR image (Figure 4D), the Umm Garaiat and Marahiq alteration zones did not show up. This image, however, is useful in showing north-trending fractures (labeled **FR** in Figure 4D) better than do the Landsat TM images (Figures 4A, 4B, and 4C). Similarly, the SIR-C/X-SAR image reveals traces of northwest-trending Neoproterozoic structure which deforms the meta-volcanic rocks hosting the massive sulfide deposits in the Wadi Marahiq area (labeled **NS** in Figure 4D). This northwest trend is similar to the orientation of the Marahiq alteration zones. In addition, the SIR-C/X-SAR image proved useful in tracing the outline of late- to post-tectonic granites (labeled **PG** in Figure 4D) which intrude the supracrustal rocks in the western part of the study area.

Density Slicing Technique

Density slicing converts the 256 shades of gray in an image into discrete intervals, each corresponding to a specific range of digital numbers (DN). Different density slices are shown as separate colors that can be draped over background images. We used this technique to create clay and iron alteration index maps of the Umm Garaiat and Marahiq alteration zones using band-ratios 5/7 (Figure 4E) and 3/1 (Figure 4F), respectively. Landsat TM band-ratio 5/7 maps clay alteration as the clay minerals such as kaolinite, montmorillonite, illite, and alunite, have reflectance maxima within Landsat TM band 5 and reflectance minima within TM band 7 (Sabins, 1997). Landsat TM band-ratio 3/1 maps iron alteration as the iron minerals such as limonite, goethite, and hematite have reflectance maxima within the visible red Landsat TM band 3 and reflectance minima within the visible blue Landsat TM band 1 (Sabins, 1997). Hence, density slicing using 5/7 and 3/1 results in clay and iron alteration index maps, respectively. This technique proved useful for identifying gossans in the Neoproterozoic terranes of northern Eritrea, where gossans are surrounded by broad zones of clay and iron alteration (Abdelsalam *et al.*, 2000a).

The clay alteration index map reveals the Umm Garaiat alteration zone as a circular structure with high concentrations of clay (Figure 4E). Similarly, this index map shows the Marahiq alteration zone coinciding with at least three anomalies (Figure 4E). The clay alteration index map also shows that the talc schist body (labeled **TA** in Figure 4A) coincides with a clay anomaly and doesn't discriminate it from the alteration zones. The iron oxide index map did not reveal significant anomalies coinciding with the Umm Garaiat and Marahiq alteration zones (Figure 4F). Instead, the anomaly coincides with weathered granite and supracrustal rocks close to the contact between the Neoproterozoic crystalline rocks and the Cretaceous sandstone (Figures 2 and 4F). The absence of iron oxide anomaly coinciding with the Umm Garaiat and Marahiq alteration zones is consistent with the fact that no gossans were observed in the field.

Supervised Classification

This technique involves selecting a pixel, individual pixels, or a cluster of pixels with known geologic significance and using these as training sites to locate regions with similar spectral characteristics (Research Systems, Inc., 1997). The Umm Garaiat alteration zone (labeled **1** in Figures 4B and 4C) was chosen as a training site for this purpose. Selection of a cluster of pixels as a training site was done on the 5/7-4/5-3/1 Landsat TM image. A cluster of 29 pixels was selected and used in a parallelepiped supervised classification based on Landsat TM band-ratios 5/7 and 3/1 using standard deviation from the mean of 2.5 to identify areas with reflectance spectra similar to the Umm Garaiat alteration zone (Figure 4G). Parallelepiped classification of multispectral remote sensing data uses algorithms whereby an *n*-dimensional parallelepiped is defined by a selected standard deviation. The classified pixels are the ones with DN values above the low threshold and below the high threshold for all bands used in the classification (Richards, 1994). This is important in geology because it allows defining the classification parameters of training sites with specific geologic meaning. The results of the parallelepiped supervised classification are remarkably similar to those obtained from the 5/7 density slicing, with the exception that the supervised classification technique succeeded in differentiating between the alteration zones and the talc schist body (compare Figure 4G with Figures 4E and 4A).

Supervised classification helped identify previously unknown alteration zones at Wadi Marahiq (Figure 4E). This exercise demonstrates the utility of density slicing and supervised classification for identifying previously unknown alteration zones and related ore deposits in the Southeastern Desert of Egypt and other arid regions. The supervised classification also showed many small areas being classified as hydrothermally altered zones (Figure 4G). We interpreted these as areas covered with weathering products from the main alteration zones outcrops now deposited on the dry-river beds (compare Figure 4G with 4A). Alternatively, these might represent previously unmapped hydrothermally altered zones. This await field confirmation.

Discussion and Conclusion

Landsat TM data have been used to map alteration zones because of their characteristic spectral properties (Abrams *et al.*, 1983; Buckingham and Sommer, 1983; Goetz *et al.*, 1983; Drury and Hunt, 1988; Kaufmann, 1988; Amos and Greenbaum, 1989; Kaufmann and Kruck, 1989; Frei and Jutz, 1989; Rockwell, 1989; Kruse, 1989; Fraser, 1991; Loughlin, 1991; Filho *et al.*, 1996; Filho and Vitorello, 1997; van der Meer, 1997; Ruiz-Armenta and Prol-Ledesma, 1998). Clay minerals such as sericite have reflectance maxima within Landsat TM band 5 (reflected IR; wavelength = 1.55 to 1.75 μm) and reflectance minima within Landsat TM band 7 (reflected IR; wavelength = 2.08 to 2.35 μm) (Hunt and Ashley, 1979). Iron minerals such as limonite and jarosite have reflectance maxima within the Landsat TM band 3 (visible red; wavelength = 0.63 to 0.69 μm) and reflectance minima within the Landsat TM band 1 (visible blue; wavelenth = 0.45 to 0.52 μm) (Hunt *et al.*, 1971). Hence, using 5/7 and 3/1 Landsat TM band-ratios effectively map clay and iron alteration zones.

This study demonstrates the importance of orbital remote sensing for identifying alteration zones and associated ore deposits in the Southeastern Desert of Egypt and other arid regions. Gold-bearing massive sulfide deposits in the Neoproterozoic Arabian-Nubian Shield are often expressed as alteration zones enriched by clay and iron minerals. Landsat TM images can be used to map the alteration zones because of their characteristic reflectance spectra. In the Wadi Allaqi area in the Southeastern Desert of Egypt, Landsat TM together with SIR-C/X-SAR images were used to identify the location and extent of the alteration zones associated with gold-bearing massive sulfide deposits which are hosted by the meta-volcanic sequences of the Neoproterozoic Allaqi suture. Landsat TM band-ratio images as well as density slicing and supervised classification techniques enabled locating the previously mapped Umm Garaiat alteration zone as well as suggesting the presence of previously unknown alteration zones in the Marahiq area that might be associated with underlying massive sulfide deposits. SIR-C/X-SAR images were not useful in locating the alteration zones, but these images were useful in understanding lithological and structural controls.

Acknowledgments

We thank three anonymous reviewers for their constructive comments. The Ministry of Scientific Research of Egypt supported work by T. Ramadan. Work by University of Texas at Dallas scientists was supported by the NASA grant through JPL #961023/97001.

References

Abdelsalam, M.G., and R.J. Stern, 1996a. Sutures and shear zones in the Arabian-Nubian Sheild, *Journal of African Earth Sciences*, 23:289–310.

———, 1996b. Mapping Precambrian structures in the Sahara Desert with SIR-C/X-SAR Radar: The Neoproterozoic Keraf Suture, NE Sudan, *Journal of Geophysical Research*, 101:23,063–23,076.

Abdelsalam, M.G., R.J. Stern, and W.G. Berhane, 2000a. Mapping gossans in arid regions with Landsat TM and SIR-C/X-SAR imagery: The Beddaho alteration zone in northern Eritrea, *Journal of African Earth Sciences*, 30:903–916.

Abdelsalam, M.G., C. Robinson, F. El-Baz, and R.J. Stern, 2000b. Applications of orbital imaging radar to geologic studies in arid regions: The Saharan testimony, *Photogrammetric Engineering & Remote Sensing*, 66(6):717–726.

Abrams, M.J., D. Brown, L. Lepley, and R. Sadowski, 1983. Remote sensing for porphyry copper deposits in southern Arizona, *Economic Geology*, 78:591–604.

Buckingham, W.F., and S.E. Sommer, 1983. Mineralogical Characterization of rock surfaces formed by hydrothermal alteration and weathering—Application to remote sensing, *Economic Geology*, 78:664–674.

Campbell, B.A., and D.B. Campbell, 1992. Analysis of volcanic surface morphology on Venus from comparison of Arecibo, Magellan, and terrestrial airborne radar data, *Journal of Geophysical Research*, 97:16293–16314.

El-Nisr, S.A., 1997. Late Precambrian volcanism at Wadi Allaqi, SE Desert, Egypt: Evidence for continental arc/continental margin environment, *Journal of African Earth Sciences*, 24:301–313.

El-Shazly, E.M., M.A. Abdel-Hady, and I.A. El-Kassas, 1983. Regional geological investigation of Wadi Allaqi area, S Egypt, from the interpretation of Landsat imagery, *Proceedings of the Seventeenth International Symposium on Remote Sensing and Environment*, Ann Arbor, Michigan, 17:703–713.

———, 1986. Gold exploration by remote sensing techniques in Wadi El Allaqi area, E Desert, Egypt, *Proceedings of the Twentieth International Symposium on Remote Sensing and Environment*, Nairobi, Kenya, 20:185–195.

———, 1988. Gold exploration by remote sensing techniques in Wadi El Allaqi area, Egypt, *Photogrammetria*, 42:303–310.

Farr, T.G., and O.A. Chadwick, 1996. Geomorphic processes and remote sensing signatures of alluvial fans in the Kun Lun Mountains, China, *Journal of Geophysical Research*, 101:23,091–23,100.

Filho, R.A., I. Vitorello, and V.R.M. Correia, 1996. Use of Landsat Thematic Mapper imagery as mineral prospecting tool in the tin province of Goias, Brazil, *Geocarto International*, 11:61–69.

Filho, R.A., and I. Vitorello, 1997. Remote sensing and field data integration in the definition of hydrothermally altered areas in vegetated terrain, central Brazil, *International Journal of Remote Sensing*, 18:1835–1842.

Frasers, J., 1991. Discrimination and identification of ferric oxides using satellite Thematic Mapper data: A Newman case study, *International Journal of Remote Sensing*, 12:635–641.

Frei, M., and L. Jutz, 1989. Use of Thematic Mapper data for the detection of gold bearing formations in the Eastern Desert of Egypt, *Proceedings of the Seventh Thematic Conference on Remote Sensing in Exploration Geology*, Calgary, Canada, pp. 1157–1172.

Greiling, R.O., M.M. Abdeen, A.A. Dardir, H. ElAkhal, M.F. El Ramly, G.M. Kamal El Din, A.F. Osman, A.A. Rashwan, A.H.N. Rice, and M.F. Sadek, 1994. A structural synthesis of the Proterozoic Arabian-Nubian Shield in Egypt, *Geologische Rundschau*, 83: 484–501.

Harris, J., 1989. Data integration for gold exploration in eastern Nova Scotia using a GIS, *Proceedings of the Seventh Thematic Conference on Remote Sensing in Exploration Geology*, Calgary, Canada, pp. 33–250.

Hume, W.F., 1937. *Geology of Egypt*, Government Press, Cario, Egypt, 990 p.

Hunt, G.R., and R.P. Ashley, 1979. Spectra of altered rocks in the visible and near infrared, *Economic Geology*, 74:1613–1629

Hunt, G.R., J.W. Salisbury, and C.J. Lenhoff, 1971. Visible and near-infrared spectra of minerals and rocks: III. Oxides and Hydroxides, *Modern Geology*, 2:195–205.

Hussein, A.A., 1990. Mineral deposits, *The Geology of Egypt* (R. Said, editor), Balkema, Rotterdam, pp. 511–566.

Kaufmann, H., and W. Kruck, 1989. Mineral exploration in the Yemen Arab Republic by use of TM-data (Preliminary results), *Proceedings of the Seventh Thematic Conference on Remote Sensing in Exploration Geology*, Calgary, Canada, pp. 1223–1227.

Kearey, P., 1993. *The Encyclopedia of the Solid Earth Sciences*, Blackwell, Oxford, 713 p.

Kruse, F.A., 1989. Spectral mapping with Landsat Thematic Mapper and imaging spectroscopy for precious metals exploration, *Proceedings of the Seventh Thematic Conference on Remote Sensing in Exploration Geology*, Calgary, Canada, pp. 15–28.

Lewis, A.J., F.M. Henderson, and D.W. Holcomb, 1998. Radar fundamentals: The geoscience prospective, *Principals and Applications of Imaging Radar* (F.M. Henderson and A.J. Lewis, editors), John Wiley and Sons, New York, N.Y., pp. 131–181.

Loughlin, W.P., 1991. Principal component analysis for alteration mapping, *Photogrammetric Engineering & Remote Sensing*, 57: 1163–1169.

Research Systems, Inc., 1997. *The Environment for Visualizing Images "ENVI," version 3.0*. Research Systems, Inc., Boulder, Colorado, 614p.

Rheault, M., R. Simard, C. Gameau, and V.R. Slaney, 1989. SAR-Landsat TM-Geophysical data integration utility of value-added products in geological exploration, *Proceedings of the Seventh Thematic Conference on Remote Sensing in Exploration Geology*, Calgary, Canada, pp. 549–559.

Richards, J.A., 1994. *Remote Sensing Digital Image Analysis*, Springer-Verlag, Berlin, 340 p.

Rockwell, B.W., 1989. Hydrothermal alteration mapping in spectral ratio feature space using TM reflectance data: Aurora Mining District, Mineral County, Nevada, *Proceedings of the Seventh Thematic Conference on Remote Sensing in Exploration Geology*, Calgary, Canada, pp. 1189–1205.

Rowan, L.C., and T.L. Bowers, 1995. Analysis of linear features mapped in Landsat Thematic Mapper and side-looking airborne radar images of the Reno 1° by 2° quadrangle, Nevada and California: Implication for mineral resource studies, *Photogrammetric Engineering & Remote Sensing*, 61(6):749–759.

Ruiz-Armenta, J.R., and R.M. Prol-Ledesma, 1998. Techniques for enhancing the spectral response of hydrothermal alteration minerals in Thematic Mapper images of central Mexico, *International Journal of Remote Sensing*, 19:1981–2000.

Sabins, F.F., 1997. *Remote Sensing Principles and Interpretation*, W.H. Freeman and Company, New York, 494 p.

Sato, T., 1974. Distribution and geological setting of the Kuroko deposits, *Geology of Kuroko Deposits* (S. Ishihara, editor), The Society of Mining Geologist of Japan Special Issue, pp. 1–9.

Singhroy, V.H., F.M. Kenny, and P.J. Barnett, 1989. Radar imagery for Quaternary geological mapping in glaciated terrains, *Proceedings of the Seventh Thematic Conference on Remote Sensing in Exploration Geology*, Calgary, Alberta, Canada, pp. 591–600.

Stern, R.J., 1994. Arc assembly and continental collision in the Neoproterozoic East African Orogen: Implications for the consolidation of Gondwanaland, *Annual Reviews of Earth and Planetary Science*, 22:319–351.

Sultan, M., R.E. Arvidson, and N.C. Sturchio, 1986. Mapping of serpentinites in the E Desert of Egypt by using Landsat Thematic Mapper data, *Geology*, 14:995–999.

Sultan, M., R.E. Arvidson, N.C. Sturchio, and E.A. Guiness, 1987. Lithologic mapping in arid regions with Landsat Thematic Mapper data: Meatiq dome, Egypt, *Geological Society of America Bulletin*, 99:748–762.

van der Meer, F., 1997. Mineral mapping and Landsat Thematic Mapper image classification using spectral unmixing, *Geocarto International*, 12:27–40.

Weeks, R.J., M. Smith, K. Pak, W. Li, A. Gillespie, and B. Gustafson, 1996. Surface roughness, radar backscatter, and visible and near-infared reflectance in Death Valley, California, *Journal of Geophysical Research*, 101(E10):23,077–23,090.

Zebker, H.A., and R.M. Goldstein, 1986. Topographic mapping from interferometric synthetic aperture radar observations, *Journal of Geophysical Research*, 9:4993–4999.

Zebker, H.A., P. Rosen, S. Hensley, and P.J. Mouginis-Mark, 1996. Analysis of active lava flows on Kilauea volcano, Hawaii, using SIR-C radar correlation measurements, *Geology*, 24:495–498.

(Received 27 June 1999; revised and accepted 25 January 00)